Journal of ELECTRONIC MATERIALS, Vol. 49, No. 9, 2020
https://doi.org/10.1007/s11664-020-08141-7

TOPICAL COLLECTION: 18TH CONFERENCE ON DEFECTS (DRIP XVIII)

Comparative Study of the Photoelastic Anisotropy of Si and GaAs

MARTIN HERMS,[1,3] GERT IRMER,[2] GREGOR KUPKA,[1] NANDO KIRCHNER,[1] and MATTHIAS WAGNER[1]

1.—PVA Metrology & Plasma Solutions GmbH., Am Nasstal 6/8, 07751 Jena-Maua, Germany. 2.—Institute of Theoretical Physics, TU Bergakademie Freiberg, 09596 Freiberg, Germany. 3.—e-mail: martin.herms@pvatepla.com

In this paper we present the results of experiments on single-crystalline (100)Si and (100)GaAs wafers which allow us to determine the degree of photoelastic anisotropy A_{pe} in the near-infrared range (probing laser wavelength $\lambda \approx 1.3$ μm). A_{pe} is introduced as the absolute value of $(\pi_{11} - \pi_{12} - \pi_{44})/(\pi_{11} - \pi_{12} + \pi_{44})$. π_{11}, π_{12} and π_{44} are the piezo-optical coefficients. The experiments were carried out using a scanning infrared depolarization imager (SIRD) measurement system equipped with special calibration setups. These setups produce a defined diametrical loading of the wafer. The different measurement and analysis strategies are explicated. The generated birefringence and shear stress equivalent maps impressively illustrate the respective opposite photoelastic properties of Si and GaAs. The experimental results are compared with simulation data on the basis of a classic 2D stress model, taking into account the crystallographic anisotropy by applying the full tensor calculus. For GaAs, A_{pe} is determined to be 0.41 ± 0.02. This value and the best-matching coefficients π_{ij} which were used for simulation are compared with data available from publications of the past few decades.

Key words: Gallium arsenide, silicon, stress-induced birefringence, piezo-optical coefficients, scanning infrared depolarization imager, diametrical wafer loading

INTRODUCTION

The distribution of stress and defects on semiconductor wafers can be analyzed as a fingerprint revealing the details of manufacturing. Infrared polaroscopy imaging, which uses the effect of stress-induced birefringence, is a fast, nondestructive and highly sensitive way to evaluate those stress states under industrial conditions. Failure analysis and process optimization on a high level are based on quantified data. This requires suitable calibration procedures.

(Received November 27, 2019; accepted April 2, 2020; published online April 26, 2020)

The scanning infrared depolarization imager (SIRD) is a fully automated transmission dark-field plane polariscope capable of fast in-line wafer mapping. The SIRD uses the phenomenon of stress-induced optical birefringence represented by the difference of the in-plane refractive indices Δn_{max}. This birefringence changes the polarization of an infrared laser beam (wavelength $\lambda \approx 1.3$ μm), resulting in a map of depolarization. One main feature of the SIRD that distinguishes it from other imaging polariscopes is the mode of wafer recording. The wafer rotates, and the scanning laser beam moves along the radius like in a disc player. Here, the measurement mode where the center of rotation and the wafer center are coincident is called "symmetrical". This enables a special calibration

procedure where the wafer is diametrically loaded by the centrifugal force of an additional movable mass.[1]

We recently demonstrated how this calibration setup could be used to determine the photoelastic constant of single-crystalline Si, wherein the dependence on the crystal orientation was exploited.[2] This photoelastic anisotropy A_{pe} was introduced as the absolute value of $(\pi_{11} - \pi_{12} - \pi_{44})/(\pi_{11} - \pi_{12} + \pi_{44})$, where π_{11}, π_{12} and π_{44} are the piezo-optical coefficients. For Si, A_{pe} was determined to be 0.21 ± 0.01. The SIRD patterns of the so-called shear stress equivalent G were simulated by applying a classic 2D stress model of diametrical loading, but using the full tensor calculus of photoelastic theory. A_{pe} was determined first by analyzing the dependence of the magnitude G on the rotation frequency near the wafer center for each loading position, but the exact knowledge of the loading force F was not necessary. Second, A_{pe} was determined by reproducing the experimental data on the G map along a selected profile called the "summit line".

We have now developed a second calibration procedure using a stretched metal wire pair, where F can be exactly adjusted by controlling the resonance vibration frequency. Therefore, we can analogously analyze the dependence of G on F in the symmetric mode. However, this setup can furthermore be used to determine the Δn_{max} distribution using the so-called eccentric procedure. This means that the wafer is shifted off the rotation center using an eccentric wafer holder. This procedure follows from the fact that plane polariscopes such as the SIRD only measure a non-zero signal if the polarization of the scanning laser is not aligned parallel or perpendicular to the principal axes of the in-plane indicatrix of n. The initial laser polarization of the SIRD is fixed in radius direction r. As a consequence, the SIRD makes Δn_{max} only partially visible according to

$$G = \frac{1}{2}\Delta n_{max}\sin(2\gamma') \tag{1}$$

γ' is the angle between the initial polarization and one of the principal axes of n. The shear stress τ is defined analogously to the optical measure G:

$$\tau = \frac{1}{2}\tau_{max}\sin(2\gamma). \tag{2}$$

Consider a 2D stress state $\sigma(x, y)$ for a simplified isotropic case as pictured schematically in Fig. 1. Then τ_{max} is given as the difference between the principal axes S_1 and S_2. For anisotropic materials such as Si and GaAs, the principal directions of the ellipses of the refractive index and stress are slightly different. As a consequence, we have to distinguish formally between γ' and γ. The angles γ and γ' can be substituted by the difference $(\phi - \theta)$ and $(\phi - \theta')$, respectively. However, for further comparison of simulated and experimental results, this distinction does not actually matter.

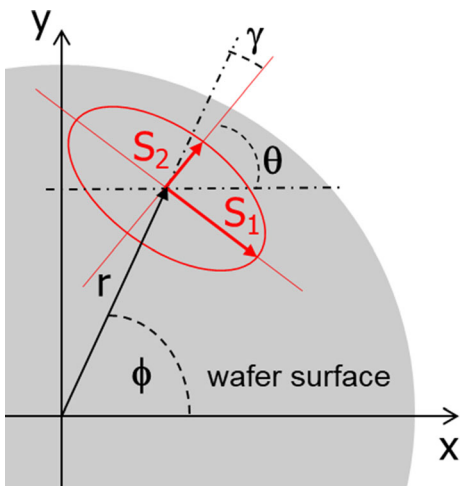

Fig. 1. Scheme illustrating the x–y coordinate system of the SIRD and the indicatrix representing the in-plane stress state for an isotropic sample without considering any crystal symmetry. S_1 and S_2 are the principal stress axes. ϕ is the angle of linear polarization aligned in the radial direction, and θ is the angle of the principal stress axes referred to the laboratory axis x. Hence, the difference $(\phi - \theta)$ defines the angle γ, which represents the resulting depolarization due to stress-induced birefringence.

In this paper we compare the results obtained for semi-insulating (100)Si and (100)GaAs wafers after applying both setups for loading. The results demonstrate the opposite photoelastic behavior of Si and GaAs. The finally determined values of A_{pe} are compared with widely varying data obtained from literature dating back to the 1950s.

THEORETICAL

This paragraph is the revision of the theoretical section in our previous article.[2] The key relation for describing the photoelastic effect in crystals is the stress-optic law:

$$\Delta B_{ij} = \sum_{k,l=1}^{3} \pi_{ijkl}\sigma_{kl}. \tag{3}$$

This law joins the stress-induced part of the change in the inverse dielectric tensor ΔB_{ij} with the tensor of stress σ_{kl}. ΔB_{ij} can be converted for small deviations into Δn_{ij}, the change in the tensor of the refractive index n. The piezo-elastic or stress-optic coefficients π_{ijkl} are linked with the strain-optic coefficients p_{ijmn} via Hooke's law according to

$$\Delta B_{ij} = \sum_{m,n=1}^{3} p_{ijmn}\varepsilon_{mn} = \sum_{m,n,k,l=1}^{3} p_{ijmn}s_{mnkl}\sigma_{kl} \tag{4}$$

with

$$\pi_{ijkl} = \sum_{m,n=1}^{3} p_{ijmn}s_{mnkl}, \tag{5}$$

where s_{mnkl} are the elastic compliance coefficients. Here we consider an extensional stress as positive for the purpose of defining the signs of π_{ijkl}. For silicon and GaAs as cubic crystals belonging to the symmetry class T_d, the stress-elastic behavior is described by the three coefficients π_{1111}, π_{1122} and π_{1212} (π_{11}, π_{12} and π_{44} in Voigt's notation). In the case of a coordinate system parallel to the fourfold symmetry axes and 2D stress state $\sigma(x,y)$ with $\sigma_x = \sigma_{11}$, $\sigma_y = \sigma_{22}$ and $\tau_{xy} = \sigma_{12}$ from Eq. 3, it follows that

$$\Delta B_{11} = \pi_{1111}\sigma_{11} + \pi_{1122}\sigma_{22} = \pi_{11}\sigma_{11} + \pi_{12}\sigma_{22} \quad (6a)$$

$$\Delta B_{22} = \pi_{1122}\sigma_{11} + \pi_{111}\sigma_{22} = \pi_{12}\sigma_{11} + \pi_{11}\sigma_{22} \quad (6b)$$

$$\Delta B_{12} = 2\pi_{1212}\sigma_{12} = \pi_{44}\sigma_{12}. \quad (6c)$$

These equations correspond to the coordinate system in Fig. 1, for example, with crystal axes $[100]||x$, $[010]||y$ and $[001]||z$. In our experiments, the wafer is fixed to the loads with different angles ϕ' between the y-axis (parallel to the load direction) and the crystallographic direction [010]. Rotation of the wafer about its [001]-axis by an angle ϕ' can be described by the directional cosine matrix α_{ij} with the elements $\alpha_{11} = \alpha_{22} = cos(\phi')$, $\alpha_{12} = -\alpha_{21} = sin(\phi')$, $\alpha_{33} = 1$ and $\alpha_{13} = \alpha_{23} = \alpha_{31} = \alpha_{32} = 0$. The stress-optic coefficients are transformed according to

$$\pi'_{ijkl} = \sum_{q,r,s,t=1}^{3} \alpha_{iq}\alpha_{jr}\alpha_{ks}\alpha_{lt}\pi_{qrst}, \quad (7)$$

and the transformed $\Delta B'_{ij}$ are

$$\Delta B'_{11} = a'\sigma_{11} + b'\sigma_{22} + 2c'\sigma_{12} \quad (8a)$$

$$\Delta B'_{22} = b'\sigma_{11} + a'\sigma_{22} - 2c'\sigma_{12} \quad (8b)$$

$$\Delta B'_{12} = c'(\sigma_{11} - \sigma_{22}) + 2d'\sigma_{12} \quad (8c)$$

with

$$a' = \pi'_{1111} = \frac{1}{4}(3\pi_{11} + \pi_{12} + \pi_{44}) + \frac{1}{4}\cos(4\phi')(\pi_{11} - \pi_{12} - \pi_{44}) \quad (9a)$$

$$b' = \pi'_{1122} = \frac{1}{4}(\pi_{11} + 3\pi_{12} - \pi_{44}) - \frac{1}{4}\cos(4\phi')(\pi_{11} - \pi_{12} - \pi_{44}) \quad (9b)$$

$$c' = \pi'_{1112} = -\frac{1}{4}\sin(4\phi')(\pi_{11} - \pi_{12} - \pi_{44}) \quad (9c)$$

$$d' = \pi'_{1212} = \frac{1}{4}(\pi_{11} - \pi_{12} + \pi_{44}) - \frac{1}{4}\cos(4\phi')(\pi_{11} - \pi_{12} - \pi_{44}). \quad (9d)$$

As can be seen, Eqs. 9 are independent of the angle ϕ' for ($\pi_{11} - \pi_{12} = \pi_{44}$). This is the condition for isotropy, and the equations are traced back to Eqs. 6.

In contrast to the special case discussed by Gamarts et al.,[3] for arbitrary angles ϕ' of the crystal orientation, the two ellipses which characterize the tensors of $\Delta B'$ and σ in the (x, y) plane are twisted against each other and against the x, y axes. The renewed transformation of Eqs. 8 and 9 to the optical principal axes provides the principal values B''_{11}, B''_{22}, n_1 and n_2.

For the shear stress equivalent G measured by SIRD we get

$$G = \frac{1}{2}\Delta n_{\max}\sin[2(\phi - \theta')] \quad (10)$$

with

$$\Delta n_{\max} = n_2 - n_1 = -\frac{n_0^3}{2}(B''_{11} - B''_{22}) = -\frac{n_0^3}{2}\sqrt{(B'_{11} - B'_{22})^2 + 4B'^2_{12}} \quad (11)$$

and

$$\theta' = \frac{1}{2}\arctan\left[2B'_{12}/(B'_{11} - B'_{22})\right]. \quad (12)$$

n_0 is the refractive index of the stressless state. At $\lambda = 1.3$ μm we use $n_0 = 3.5$[4] for Si and 3.4[5] for GaAs.

Measurements near the wafer center allow direct access to the anisotropy determination. In this case we have vanishing shear stress $\sigma_{12} = \tau_{xy} = 0$. $\sigma_{11} = \sigma_x$ and $\sigma_{22} = \sigma_y$ are the principal stress values (see Eq. 16), and we obtain

$$\Delta n_{\max} = -\frac{n_0^3}{2}\sqrt{(\pi_{11} - \pi_{12})^2\cos^2(2') + \pi_{44}^2\sin^2(2')}(\sigma_x - \sigma_y). \quad (13)$$

The methodology of diametrical loading for testing cylindrical samples and for calibrating photoelastic experimental setups has been given in several textbooks.[6–8] Hence, in the past this experimental strategy was applied to measure the photoelastic properties of silicon and GaAs wafers.[9–11]

As already introduced, the general case of a two-dimensional stress state $\sigma(x, y)$ can be pictured as an ellipse represented by two principal half-axes S_1 and S_2 which are turned to y and x, respectively, by θ:

$$\theta = \frac{1}{2}\arctan[2\tau_{xy}/(\sigma_x - \sigma_y)]. \quad (14)$$

The shear stress maximum τ_{max} is the most relevant quantity for our method, since it can be converted to Δn_{max} and vice versa. It is given by

$$\tau_{max} = \frac{1}{2}\Delta\sigma_{max} = \frac{1}{2}(S_1 - S_2) = \frac{1}{2}((\sigma_x - \sigma_y)^2 + 4\tau_{xy}^2)^{1/2}. \quad (15)$$

The analytical model of stress $\sigma(x, y)$ for a diametrically loaded circular disc has been derived e.g. by Frocht[12] and Timoshenko.[13] This model yields relations for $\sigma_x(x, y)$, $\sigma_y(x, y)$ and $\tau_{x,y}(x, y)$ which show a linear dependence on the loading force F. R is the wafer radius and d is the wafer thickness.

$$\sigma_x = -2F/\pi d\{\{[(R-y)x^2]/[x^2+(R-y)^2]^2 + [(R+y)x^2]/[x^2+(R+y)^2]^2\} - 1/2R\} \quad (16a)$$

$$\sigma_y = -2F/\pi d\{\{[(R-y)^3]/[x^2+(R-y)^2]^2 + [(R+y)^3]/[x^2+(R+y)^2]^2\} - 1/2R\} \quad (16b)$$

$$\tau_{xy} = -2F/\pi d\left\{-[(R-y)^2x]/[x^2+(R-y)^2]^2 + \left[(R+y)^2x]/[x^2+(R+y)^2\right]^2\right\}. \quad (16c)$$

EXPERIMENTAL

The special procedure for SIRD calibration which uses the rotation for generating defined centrifugal force was already presented in brief in 2013.[1] Figure 2a shows the scheme of the wafer holder equipped with two diametrically positioned masses, one movable and one fixed, which load a defined centrifugal force F_c via a lever on the wafer edge. Hence, the loading force F has a linear dependence on the squared frequency of rotation ω_{rot}. β_1 is a device-specific transmission factor.

$$F = \beta_1\omega_{rot}^2 \quad (17)$$

For wafers of different diameter (here 6-inch GaAs and 8-inch Si), two setups with different β have been used.

Secondly, we designed an alternative setup consisting of two guitar strings which are stretched nearly equally on the front and back of the wafer (Fig. 2b). The strings are stretched by screws. The tensile force is precisely adjusted by measuring the frequency of vibration f_{string} (Eq. 18) which is excited by an electric coil using a function generator.

$$F \approx 8L^2m^*f_{string}^2 \quad (18)$$

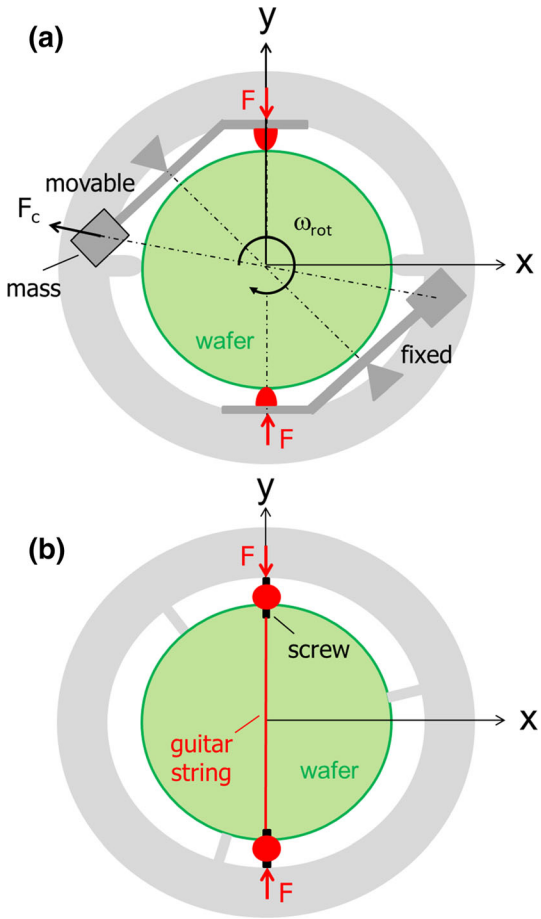

Fig. 2. Schemes of setups for calibrating SIRD by diametrical loading of the wafer. The loading force F is adjustable either by setting the rotation frequency ω_{rot} (a) or by tuning the string resonance frequency f_{string} (b).

Equation 18 follows from Taylor's relation. L is the length and m^* the mass per length of the string. The wafer prepared in this way is measured both symmetrically and eccentrically.

The symmetric experiments supply maps of the shear stress equivalent G measured at different ω_{rot} and f_{string}, respectively. The map measured at very low ω_{rot} is called the G_0 map and represents the residual stress state of the wafer without external loading.

In order to determine A_{pe}, the wafer is loaded at different preferential positions. These are the [100] and [110] orientations as well as the position at 22.5° in between. For these cases, Eq. 10 can be simplified and the situation in the wafer center approximated to:

$$G(r \approx 0) \sim -n_0^3[(\pi_{11} - \pi_{12})\cos^2(2\phi') + \pi_{44}\sin^2(2\phi')](F/\pi dR). \quad (19)$$

Hence, for the three positions of loading we get:

$$G(F@[100]) \sim -n_0^3(\pi_{11} - \pi_{12})(F/\pi dR) \quad (20a)$$

$$G(F@22.5^\circ) \sim -\frac{1}{2} n_0^3 (\pi_{11} - \pi_{12} + \pi_{44})(F/\pi dR) \tag{20b}$$

$$G(F@[110]) \sim -n_0^3 \pi_{44} (F/\pi dR). \tag{20c}$$

Consequently, A_{pe} can be determined from the slopes of the linear dependence of G on F according to:

$$A_{pe} = [\Delta G(F@[100])/\Delta F] - \Delta G(F@[110])/\Delta F]/[\Delta G(F@[100])/\Delta F + \Delta G(F@[110])/\Delta F] \tag{21a}$$

and

$$[\Delta G(F@[22.5^\circ])/\Delta F] = \frac{1}{2}[\Delta G(F@[100])/\Delta F] + \Delta G(F@[110])/\Delta F]. \tag{21b}$$

The aim of the eccentric measurement procedure is to determine Δn_{max} by eliminating the dependence of G on the angle γ (see Eq. 1). For this purpose the wafer is shifted off the rotation center. For diametrical loading, the devices for loading have to be firmly connected to the wafer. Wafer and strings rotate conjointly. A set of single maps is recorded where the wafer-string setup is turned each time by a certain angle (e.g. 20°). Hence, each point on the wafer is measured at different γ. Thus, the map of Δn_{max} can be calculated from a set of these single maps by fitting the $\sin(2\gamma)$ dependence in each point of the wafer. For each position of loading ([100], [110] and 22.5° in between), only one identical force is adjusted.

RESULTS

Figure 3 shows maps of the shear stress equivalent G which were recorded on an 8-inch (100)Si and a 6-inch (100)GaAs wafer. The wafers were diametrically loaded at three positions at the wafer edge using different centrifugal setups for wafers of different diameter. The arrows mark the position of the notch which is aligned at the Si wafer edge in the [110] direction and on GaAs in the [100] direction. To eliminate the residual stress state without loading, the maps of G_0 measured using the lowest rotation frequency were subtracted. The loading power F was estimated by comparing G measured analogously using the string setup (see Fig. 4). This means that the measurements using the centrifugal and string setups have qualitatively and quantitatively the same maps. However, the different transmission factors of the centrifugal setups hinder a direct quantitative comparison of the maps of Si and GaAs. Nevertheless, the opposing properties of Si and GaAs are obvious. The patterns of the Si wafer loaded in the [100] and [110] directions are qualitatively congruent with the patterns of the GaAs wafer loaded in the [110] and [100] directions, respectively. The blue and red branches in the 22.5° maps are asymmetric. The intensity distributions are opposite.

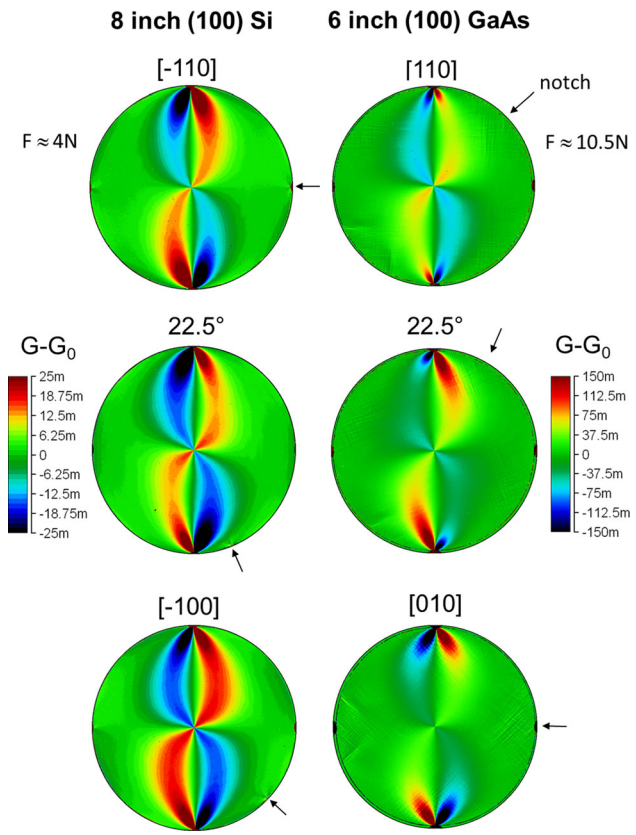

Fig. 3. Maps of the shear stress equivalent G measured using the centrifugal setups for diametrical (vertical) loading of a Si and a GaAs wafer in comparison. G_0 is the shear stress equivalent measured using the lowest rotation frequency representing the residual stress state without loading. The loading power F is estimated by comparing G measured using the string setup. The different transmission factors of the centrifugal setups do not allow a direct quantitative comparison of Si and GaAs. The arrows mark the position of the notch which is aligned at the Si wafer edge in the [110] direction and on GaAs in the [100] direction.

In a next step we have analyzed the dependence of G on F by charting G_{max}—the maximum G near the wafer center—versus the rotation frequency ω_{rot} and the resonance string frequency f_{string}, respectively. The results for GaAs are shown in Fig. 4a and b. G_0 is the G value taken from the maps near the wafer center measured without loading. ω_{max} is the maximum rotation frequency used here but not disclosed. The loading force F is estimated for the string setup by applying Eq. 18 to the data of resonance frequency determination. Consequently, each measured G value can be assigned to a related value of F if reasonable.

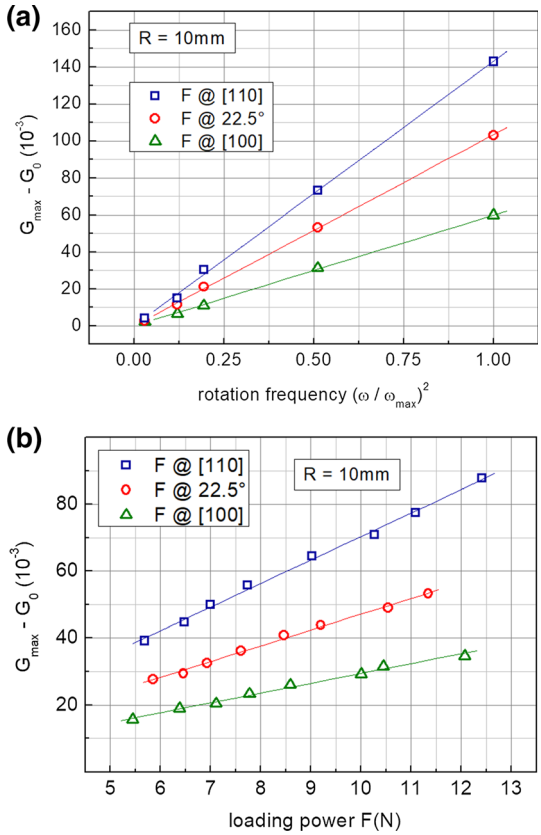

Fig. 4. Dependence of the measured shear stress equivalent G on the squared wafer rotation frequency ω_{rot} (a) and on the loading power F converted from the string resonance frequency (b) for three positions of loading on a (100)GaAs wafer. The G values were taken on the nearly flat part of the "summit line" close to the wafer center. G_0 was recorded using the lowest rotation frequency ω_{rot} and without loading respectively. ω_{max} is the maximum rotation frequency here used. The lines are linear fits.

Si and GaAs show roughly reversed values of π_{44} and $(\pi_{11} - \pi_{12})$. Hence, if we ignore the absolute value function in the definition of A_{pe}, for GaAs the degree of anisotropy is expected to be negative in contrast to Si ($A_{pe} = +0.21 \pm 0.01$; see Ref. 2). According to Eq. 22a, A_{pe} was determined to be $(-)0.41 \pm 0.02$ from the data shown in Fig. 4a (centrifugal setup) and to $(-)0.41 \pm 0.04$ from the data shown in Fig. 4b (string setup). Then this value was used to start the simulation of the G maps on the basis of sets of piezo-optical coefficients π_{44} and $(\pi_{11} - \pi_{12})$, which corresponds approximately to data available from the literature [14–17] (see Fig. 5). As already demonstrated for Si in Ref. 2, an efficient way for fitting experimental and simulated results is the comparison of the maximum G values along one of the branches—the so-called summit line. This is demonstrated now for GaAs in Fig. 6, which shows only data for the experiment using the centrifugal setup. We have refrained from adding experimental data for the $-22.5°$ loading position which are only available from the experiment using the string setup (see below). The best match was

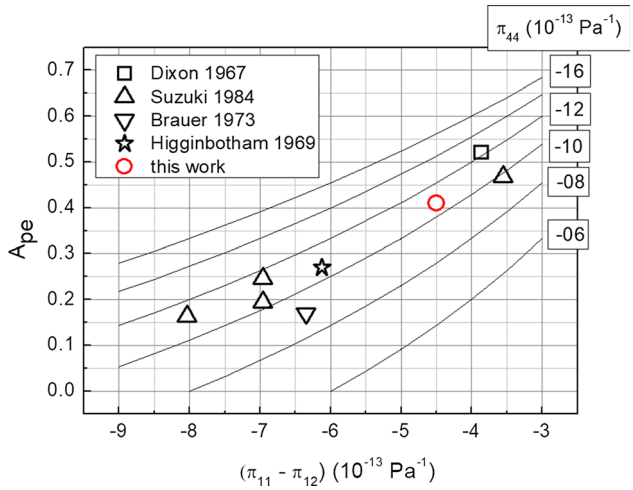

Fig. 5. The anisotropy degree A_{pe} as a function of the piezo-elastic coefficients $(\pi_{11} - \pi_{12})$ calculated in a range delimited by data from the literature.[14–17] The solid curves give the second coefficient π_{44} as a parameter.

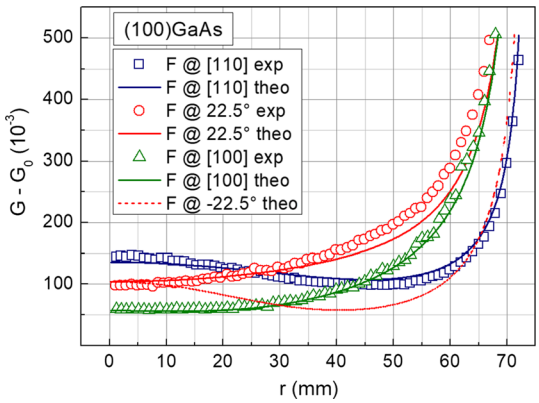

Fig. 6. Comparison of measured and calculated profiles of the shear stress equivalent $G(r, \phi)$ taken along the maximum magnitude ("summit") line in the first quarter of map (see Fig. 3, right side) for three loading positions and measured at the highest rotation frequency ω_{rot}. G_0 was recorded using the lowest ω_{rot}.

obtained for $\pi_{44} = -10.75 \times 10^{-13}$ Pa^{-1} and $(\pi_{11} - \pi_{12}) = -4.5 \times 10^{-13}$ Pa^{-1}.

Figure 7 shows the Δn_{max} maps simulated according to the theory as explicated before (Eq. 11) and experimentally obtained using the eccentric measurement procedure applied to an 8-inch (100)Si wafer. Theory and experiment are in good agreement. The anisotropy of birefringence is clearly visible.

In contrast, Fig. 8 shows the Δn_{max} maps experimentally generated on (100)GaAs and the attempt to reproduce this result by simulation. For loading F in the $[\bar{1}10]$ and [010] directions, respectively, we clearly see a distribution which is inverse to that observed for (100)Si. For loading F in the [010] direction, the splitting into two branches is much more pronounced than that observed for Si (see Fig. 7). The case in the middle figure does not seem to be different, but actually in this experiment the GaAs wafer was loaded in the $-22.5°$ direction. For

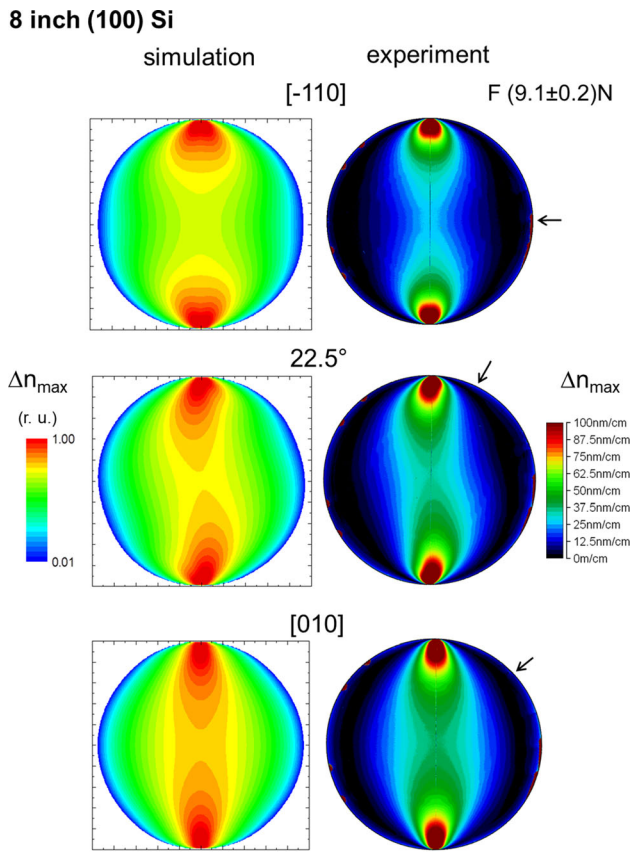

Fig. 7. Comparison of simulated and experimentally obtained maps of Δn_{max} for three positions of diametrical loading of an 8-inch (100)Si wafer. The simulation was performed according to Eq. 11 (please note the logarithmic scale). The experimental maps were generated from single maps which were recorded using the eccentric measurement mode and the string setup for loading. The arrows mark the notch position in the [110] direction.

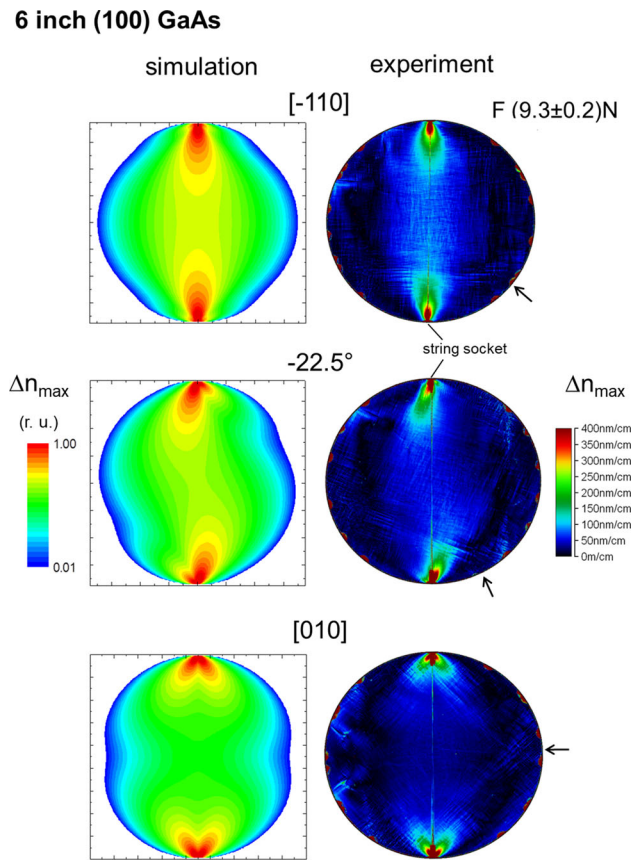

Fig. 8. Comparison of simulated and experimentally obtained maps of Δn_{max} for three positions of diametrical loading of a 6-inch (100)GaAs wafer. The simulation was performed according to Eq. 11 (please note the logarithmic scale). The experimental maps were generated from single maps which were recorded using the eccentric measurement mode and the string setup for loading. The arrows mark the notch position in the [100] direction.

all three experimental maps, the birefringence induced by diametrical loading is superimposed by pronounced slip-line patterns in the [110] direction. Therefore, for an adequate presentation, a high upper limit of scale was chosen.

SUMMARY

The photoelastic properties of single-crystalline GaAs have been comparatively investigated by means of the SIRD system equipped with two setups for diametrical loading and applying two measurement strategies. The experimental result of the symmetric measurement procedure analyzing the shear stress equivalent dependent on the loading force is the degree of anisotropy A_{pe}. For GaAs, A_{pe} was proven to be significantly higher than that for Si. The experimental results were well confirmed by simulation of full wafer maps of the load-induced G and Δn_{max}. They demonstrate the inverse character of anisotropy of (100)Si and (100)GaAs with respect to the main crystallographic axes. The difference in loading at 22.5° and −22.5° is clearly revealed but is negligible near the center area of the wafer. The maps of the studied GaAs wafer were superimposed by a pronounced defect-induced birefringence. Consequently, further experiments should be carried out on material of lower defect density.

REFERENCES

1. H.D. Geiler, K. Schulz, and R. Knechtel, *Microsyst. Technol.* 19, 697 (2013).
2. M. Herms, G. Irmer, G. Kupka, and M. Wagner, *Phys. Status Solidi A* 216, 1900254 (2019).
3. E.M. Gamarts, P.A. Dobromyslov, V.A. Krylov, S.V. Prisenko, E.A. Jakushenko, and V.I. Safarov, *J. Phys. III France* 3, 1033 (1993).
4. V.Y. Mendeleyev, S.N. Skovorodko, E.N. Lubnin, and V.M. Prosvirikov, *Appl. Phys. Lett.* 93, 131916 (2008).
5. A.D. Rakić and M.L. Majewski, *J. Appl. Phys.* 80, 5909 (1996).
6. M.M. Frocht, *Photoelasticity*, Vol. 2 (London: Wiley, 1941), p. 352.
7. J.W. Dally and W.F. Riley, *Experimental Stress Analysis*, 3rd ed. (New York: McGraw-Hill, 1991), p. 457.
8. H. Wolf, *Spannungsoptik*, Vol. 1 (Berlin: Springer, 1976), p. 78.
9. P.K. Ajmera, B. Huner, A.K. Dutta, and C.S. Hartley, *Appl. Opt.* 27, 752 (1988).
10. A.K. Dutta, P.K. Ajmera, and B. Huner, *J. Appl. Phys.* 65, 5230 (1989).

11. G. Horn, J. Lesniak, T. Mackin, and B. Boyce, *Rev. Sci. Instrum.* 76, 045108 (2005).
12. M.M. Frocht, *Photoelasticity II* (London: Wiley, 1941), p. 126.
13. S. Timoshenko and J.N. Goodier, *Theory of Elasticity* (New York: McGraw-Hill Book Company Inc., 1951), p. 107.
14. R.W. Dixon, *J. Appl. Phys.* 38, 5149 (1967).
15. N. Suzuki and K. Tada, *Jpn. J. Appl. Phys.* 23, 1011 (1984).
16. K.H. Brauer, J. Feuerstake, F. Fröhlich, and U. Mohr, *Kristall und Technik* 8, 253 (1973).
17. C.W. Higginbotham, M. Cardona, and F.H. Pollak, *Phys. Rev.* 184, 821 (1969).